Geometric Modeling of Detonation Propagation and Re-Initiation over Obstacles

Reza Paknahad, Jackson Crane
Department of Mechanical and Materials Engineering, Queen's University
Kingston, Ontario, Canada

1 Introduction

Numerical simulations remain a robust approach to study the propagation of detonations. Due to its multidimensional and transient nature, detonation propagation involves complex processes, such as shock-reaction coupling, re-initiation and failure mechanisms, and response to geometric confinement. To resolve all detonation physics, high spatial and temporal resolutions as well as detailed chemical kinetics are needed, which result in significant computational costs. Moreover, such simulations are often accompanied by inaccuracies when the physics is partially resolved [1]. An alternative to such expensive numerical simulations can be inexpensive modeling approaches that are based on the physical characteristics of detonations. One such approach is Crane et al.'s geometric model [2]. The geometric model is based on a physical understanding of the detonation wave structure. Following a series of initial blasts, the model tracks blast fronts and initiates new ignitions from blast intersections. One-dimensional (1D) cylindrical blast simulations are required to capture the locations of the blast front and the reaction front as functions of time and the initial radius of the blast for a specific mixture. The geometric model uses the simulation results as input to update the detonation structure at each time step.

The propagation of multidimensional detonations consists of a series of failures and re-initiations resulting from the interaction of Mach stems, incident shocks, and transverse waves. This complex physical behavior is represented by the detonation cellular structure. Recent studies have shown that the detonation cell size and the appearance of its cellular structure are mainly affected by chemistry and geometry [3]. When the geometric configuration is filled with obstacles, the detonation propagation can be affected in several ways. Due to momentum and heat transfer losses to the obstacle, the detonation might be suppressed. On the other hand, wave reflections off obstacles can generate local hot spots, leading to detonation re-initiation at a distance from the obstacle. The shape and arrangement of the obstacles, including their blockage ratio, have been found to affect the detonation cellular structure downstream of the obstacle [4].

In this work, we employ Crane et al.'s geometric model to study detonation propagation over obstacles in a two-dimensional (2D) channel. A blast-tracing algorithm is added to the model to trace the blast fronts and eliminate the possibility of blast propagation through the obstacle. The primary goal is to investigate how the presence of the obstacles affects detonation cellular structure, frontal velocity profiles, and possible detonation re-initiation. The accuracy and cost of the geometric model will be evaluated

Correspondence to: reza.paknahad@queensu.ca

in this context. For an initial evaluation of the model, detonation propagation over a forward-facing wedge-shaped obstacle has been tested. Numerical soot foils and mean shock velocity variations along the channel are reported for the test case. The results show that the extended geometric model can successfully simulate blast propagation and reflection over obstacles. However, the current model handles detonation re-initiation after the obstacle merely based on the deceleration of the blast waves. To capture the re-initiations based on the diffraction process, a cell generation mechanism is to be implemented into the geometric model. Experiments and detailed numerical simulations are currently underway to replicate the simulated condition in a quasi-2D channel, and will be used for direct comparison and validation purposes.

2 Methods and Results

The geometric model consists of an inner solution and an outer solution. The inner solution numerically solves the Euler equations in cylindrical coordinates in 1D, initialized from a point blast. The outputs of the inner solution are the positions of the pressure front and the temperature front as functions of time and the initial blast kernel size for a specific mixture, tabulated as lookup tables. The outer solution is analytic in space and discrete in time. It follows a series of initial blasts of different sizes and uses the inner solution tables to track the blast fronts at each time step. As the solution progresses in time, the model generates new ignitions from three intersecting blasts. This approach results in an evolving detonation cellular structure within a confined space. All blast-blast and blast-boundary intersections, including blast-obstacle intersections, are calculated using analytical geometric relations. More information on the geometric model can be found in [2, 5].

1D cylindrical blast simulations have been conducted to produce the inner solution tables. ASURF-Parallel has been used to perform the simulations. The code utilizes the finite volume method (FVM), a Riemann shock-capturing scheme, multi-level dynamically adaptive mesh refinement (AMR), and a domain decomposition method for parallel computing. More information on ASURF-Parallel can be found in [6, 7]. The simulation setup for the inner solution is as follows. The simulations have been carried out in 1D cylindrical coordinates. The domain size and the maximum number of grid points are 50 mm and 50,000 in radius, respectively. At the center of the domain (R = 0), the reflective boundary condition has been applied, while at the outer boundary (R = 50 mm), an outlet boundary condition is used. The chemical mixture in all simulations is stoichiometric hydrogen-oxygen at an initial pressure of 15 kPa and an initial temperature of 300 K. The Foundational Fuel Chemistry Model Version 1.0 (FFCM-1) is used for chemistry.

Each simulation was initiated by an initial blast with a finite kernel size and a fixed post-shock state. In this work, the initial blast post-shock state corresponds to a pressure ratio of 94.35 and a temperature ratio of 16.75 as compared to the initial conditions. These values come from the theoretical analysis of a triple-shock configuration immediately after a new detonation cell is formed. This initial condition is more representative of the thermodynamic state encountered in the detonation kernel as compared to the initial conditions proposed in Crane et al.'s original work [2]. Additional details of this analysis will be included in subsequent publication due to length restrictions. To produce the inner solution tables, different kernel sizes have been considered for the initial blast in the simulations, from 0.05 mm to 2.0 mm.

The results of the inner solution simulations are shown in Figure 1. Figure 1(a) shows pressure spatial profiles at the simulation time of t = 2 µs, and Figure 1(b) depicts temperature spatial profiles at t = 10 µs, both as functions of the radial distance from the origin, R, and the initial blast kernel size, r_0. It can be seen that as r_0 increases, stronger blast waves are formed following the initiation. Stronger blast waves exhibit higher values of pressure and temperature across the shock and higher shock velocities.

The radial positions of the pressure front, R_{P}, and the temperature front, R_{T}, as functions of t and r_0 are shown in Figure 1(c). The pressure front is defined as the shock front, and the temperature front is the position of the maximum temperature gradient behind the shock. It can be seen that as r_0 increases, pressure and temperature fronts decouple later in time, representing stronger blast waves with stronger shock-reaction coupling. Figure 1(c) is a demonstration of the inner solution tables in the geometric model. Overall, the similar trends observed in the inner solution results in Figure 1 indicate that the proposed initial blast post-shock conditions will perform similarly as compared to the original inner solution from Crane et al.'s work [2].

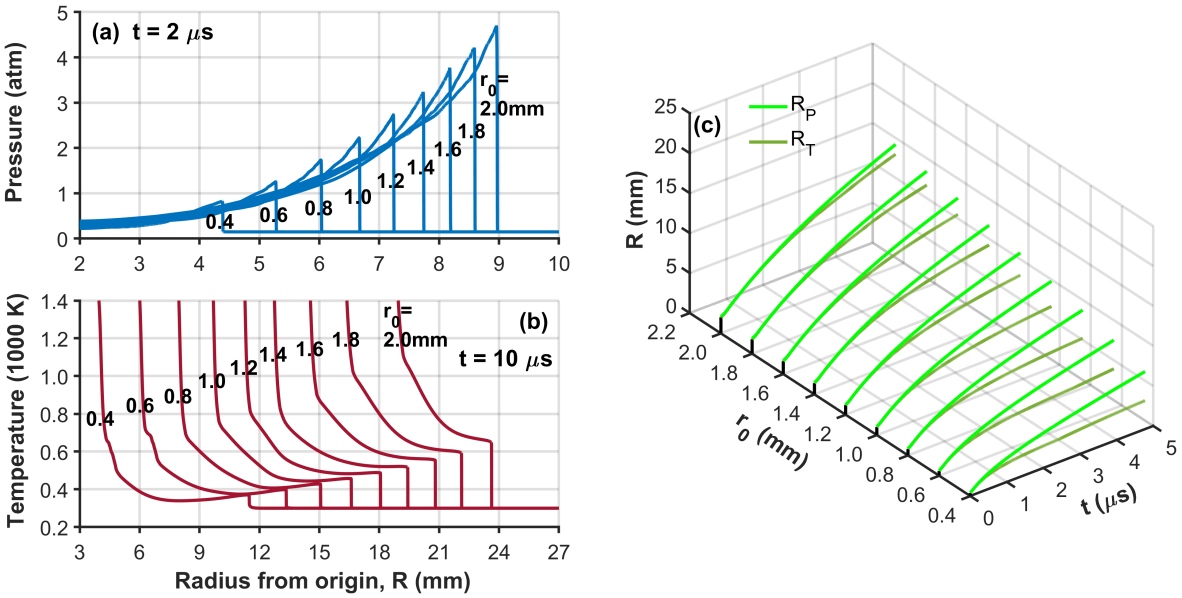

Figure 1: Results of the inner solution simulations; Pressure spatial profiles (a) at t = 2 µs and temperature spatial profiles (b) at t = 10 µs as functions of the radial distance from the origin, R, and the initial blast kernel size, r_0; The Radial positions of pressure front, R_{P}, and temperature front, R_{T}, (c) as functions of time, t, and the initial blast kernel size, r_0.

The outer solution models each blast as a circle and looks for possible blast-blast and blast-boundary intersections using the geometric relations of circle-circle and circle-line-segment intersections, respectively. The positions of the pressure front and the temperature front of each blast are updated at each time step by looking up to the inner solution tables. When three blasts intersect, including two side blasts and one center blast, a new blast is generated. The initial radius of the new blast is determined by the decoupling between the pressure and temperature fronts of the center blast. To ensure that a physical detonation propagation-reflection behavior is modeled over an obstacle, a blast-tracing algorithm is added to the geometric model. The algorithm traces the blast fronts and eliminates the possibility of blast propagation through the obstacle by removing the intersections that are formed from such blasts. The blast-tracing approach is illustrated in Figure 2 for a blast-blast intersection. All intersections (e.g., Int. a and Int. b in Figure 2) are traced from the center of their parent blasts (Blast 1 and Blast 2 in Figure 2) by connecting rays. If a ray intersects with an obstacle, the model deletes the corresponding intersection. The same algorithm applies to blast-boundary intersections but is not pictured for clarity.

To test the extended geometric model, a 2D channel filled with a forward-facing wedge-shaped obstacle has been considered (see Figure 3). The channel is long enough to ensure a steady cell structure before reaching the obstacle, while its width is 10 mm. The obstacle begins at a distance of 111 mm and is 20 mm long. Two obstacle geometries with width sizes of 2 and 4 mm have been tested, resulting in maximum blockage ratio values of 0.2 and 0.4, respectively. The blockage ratio, BR, is defined as the ratio between the obstacle width and the channel width. A reflective boundary condition was used on

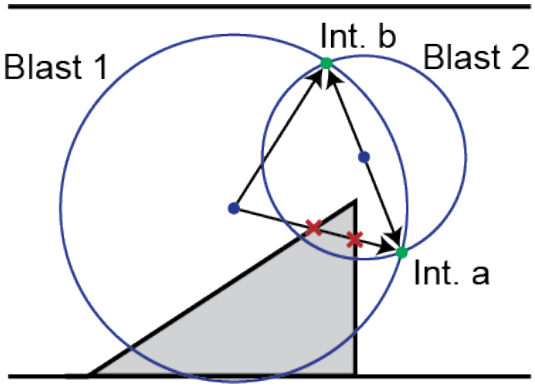

Figure 2: A schematic showing the geometric model blast-tracing algorithm, which traces rays between blast centers and blast-blast intersections and removes intersections that propagate through the obstacle.

the walls of the channel and the obstacle, which reflects a blast of equal properties once a blast intersects with a wall.

Figure 3 shows the results of the geometric model solution over the obstacles. The numerical soot foils for detonation propagation over the obstacles with $BR_{\max}$ of 0.2 and 0.4 can be seen in Figures 3(a) and 3(b), respectively. The Gaussian-smoothed mean shock velocity profiles for the soot foils are shown in Figure 3(c). Once the blast waves reach the obstacle, the effective area for detonation propagation is reduced, which eventually blocks wave reflections and leads to significant attenuation of the propagating blasts. From the shock velocity profiles, it can be seen that the area reduction results in a velocity spike at about t = 50 µs, which is sharper in the case with $BR_{\max} = 0.4$ due to larger area reduction. This acceleration is consistent with experimental observation of detonations overdriven by area reductions (e.g., [8]). The velocity spike is followed by a sudden drop in the shock velocity, leading to detonation attenuation due to the sudden expansion, similar to the critical tube diameter problem [9]. In the case with $BR_{\max} = 0.2$, there is a re-initiation at t = 58 µs, but the detonation ultimately fails, while in the case with $BR_{\max} = 0.4$, the detonation promptly fails. It can be seen that the geometric model cannot resolve the re-initiation process after the obstacle, and simply predicts deceleration of the blast waves, while previous studies exhibit re-initiation in certain cases [10]. In order to fully capture the diffraction process after the obstacle, a cell generation mechanism must be implemented into the geometric model, which is underway. Experiments and numerical simulations to directly replicate these conditions are also underway. Overall, the initial physics depicted in these simulations replicates, at and shortly after the obstacle, what is expected, based on past literature, from detonations propagating over blockages.

3 Conclusions

The detonation geometric model introduced in the work of Crane et al. [2] is extended to account for detonation propagation over obstacles. To produce the input data of the geometric model, 1D cylindrical blast simulations are performed to track the blast front and the reaction front as functions of time and the initial radius of the blast for stoichiometric hydrogen-oxygen. The simulation results are in good agreement with what is expected from cylindrical blasts of different initial sizes. The geometric modeling begins with a series of initial blasts of varying sizes and utilizes the simulation results to update the evolving detonation structure at each time step. New blasts are generated from the intersections of three blasts, and all intersections are calculated using geometric relations. A new blast-tracing algorithm is added to the model, which traces rays between blast centers and intersections and removes intersections that are created from blast propagation through the obstacle. To test the extended model, a 2D channel

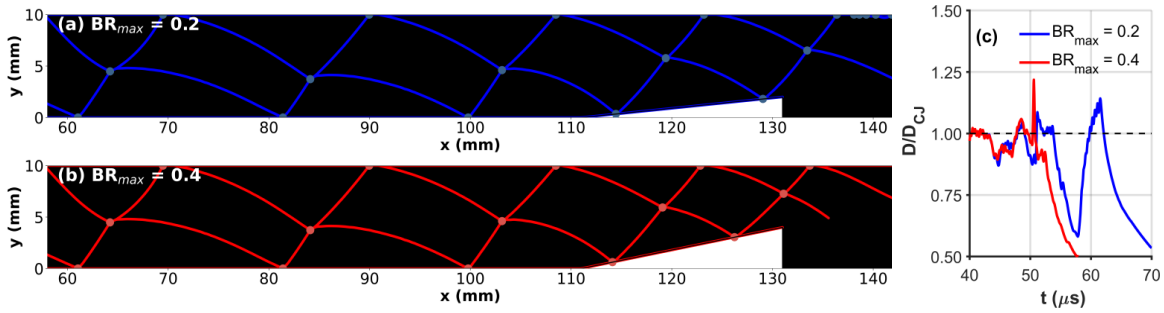

Figure 3: Test results for the extended geometric model; Numerical soot foils for detonation propagation over the obstacles with maximum blockage ratio, $BR_{\max}$, of 0.2 (a) and 0.4 (b); Gaussian-smoothed mean shock velocity profiles (c) normalized by the CJ velocity, D/D_{CJ}, for the soot foils.

filled with a forward-facing wedge-shaped obstacle is considered. Two obstacle geometries with maximum blockage ratios of 0.2 and 0.4 are studied. The test results, including numerical soot foils and mean shock velocity profiles, show good agreement with previous observations of detonations encountering obstacles. However, the current geometric model handles the re-initiation after the obstacle based on the deceleration of the front, not based on the diffraction process that has been observed in previously published data. For the final presentation, the future work includes validation/verification of the extended geometric model against new experiments and simulations, and implementing a cell generation mechanism to capture detonation diffraction after the obstacle.

References

[1] Radulescu MI. (2018). A detonation paradox: Why inviscid detonation simulations predict the incorrect trend for the role of instability in gaseous cellular detonations? Combust. Flame 195: 151-162.

[2] Crane J, Shi X, Lipkowicz JT, Kempf AM, Wang H. (2021). Geometric modeling and analysis of detonation cellular stability. Proc. Combust. Inst. 38: 3585-3593.

[3] Monnier V, Rodriguez V, Vidal P, Zitoun R. (2022). An analysis of three-dimensional patterns of experimental detonation cells. Combust. Flame 245: 112310.

[4] Li J, Pan J, Jiang C, Jin J. (2024). Effects of obstacle arrangement on the diffraction and subsequent reflection characteristics of cellular detonation across an obstacle. Int. J. of Hydrogen Energy 64: 535-547.

[5] Shi X, Hencel R, Crane J, Fotia M, Wang H. (2025). Geometric stability of detonation propagation in curved channels. Shock Waves: 1-11.

[6] Shi X, Chen JY, Chen Z. (2016). Numerical study of laminar flame speed of fuel-stratified hydrogen/air flames. Combust. Flame 163: 394-405.

[7] Chen Z, Burke MP, Ju Y. (2009). Effects of Lewis number and ignition energy on the determination of laminar flame speed using propagating spherical flames. Proc. Combust. Inst. 32: 1253-1260.

[8] Zangene F, Radulescu MI. (2024). The critical conditions for the re-ignition and detonation formation from Mach reflections of curved decaying shocks. Proc. Combust. Inst. 40: 105774.

[9] Knystautas R, Lee JH, Guirao CM. (1982). The critical tube diameter for detonation failure in hydrocarbon-air mixtures. Combust. Flame 48: 63-83.

[10] Shi X, Pan J, Jiang C, Li J, Zhu Y, Quaye EK. (2022). Effect of obstacles on the detonation diffraction and subsequent re-initiation. Int. J. of Hydrogen Energy 47: 6936-6954.